Melt Processable Conducting Poly(aniline-*co*-*o*-anisidine)/ Linear Low-Density Polyethylene Composites with Ethylene-Acrylic Acid Copolymer as Compatibilizer

Gengchao Wang, Zhongyuan Shen, Xingwei Li, Chunzhong Li

Key Laboratory for Ultrafine Materials of Ministry of Education, School of Materials Science and Engineering, East China University of Science and Technology, Shanghai 200237, People's Republic of China

Received 22 January 2005; accepted 30 March 2005
DOI 10.1002/app.21972
Published online in Wiley InterScience (www.interscience.wiley.com).

ABSTRACT: Conducting composites of aniline/*o*-anisidine copolymer doped by dodecylbenzenesulfonic acid (P(An-*co*-oAs)-DBSA), linear low-density polyethylene (LLDPE), and ethylene–acrylic acid copolymer (EAA) as compatibilizer were prepared by melt processing. The effects of composition on electrical conductivity, resistivity-temperature characteristic, and mechanical properties were also investigated. The electrical conductivity of ternary composites markedly increased due to compatibilizition and protonation effect of the EAA. The SEM micrograph shows that the compatibility between the P(An-*co*-oAs)-DBSA and the LLDPE matrix is enhanced after the introduction of EAA. The positive temperature coefficient of resistivity characteristic is observed. Tensile strength of P(An-*co*-oAs)-DBSA/LLDPE/EAA composites is improved, compared with P(An-*co*-oAs)-DBSA/LLDPE composites. © 2005 Wiley Periodicals, Inc. J Appl Polym Sci 98: 1511–1516, 2005

Key words: conducting polymer; polyethylene; melt processing; compatibilization; electrical properties

INTRODUCTION

Polyaniline (PAn) is a promising conducting polymer for practical applications because of its straightforward polymerization, good environmental stability, and high electrical conductivity.[1] However, the main disadvantage of conducting PAn, like others ICPs, is its intractable nature, especially in the doped form. Some methods have been introduced to improve solubility of PAn, such as ring substitution,[2,3] N-alkylation,[4,5] and protonation with functionalized protonic acids[6–11] With the amelioration of solubility of PAn, the techniques based on dispersion of conducting PAn in a matrix constituted by conventional insulating polymers have received more attention.[12,13] Several conducting composites of PAn with host-insulating polymers, which are prepared by melted process, have been recently reported.[14–18] Among all conducting composites of PAn with host-insulating polymers, the composite of PAn with linear low-density polyethylene (LLDPE) is very attractive because of its excellent processability, transparence, and good mechanical properties. In addition, melt processing with LLDPE can be performed at a temperature that is not so high as to cause degradation of PAn. However, the compatibility of LLDPE and conducting PAn is not very good, and the separation of phases still exists. Studies indicate that the miscibility of PAn and LLDPE can be improved by the introduction of a compatibilizer. In addition, the compatibility also is significant when the PAn– dodecylbenzenesulfonic acid (DBSA) conducting complex contains an excess of DBSA.[15,19,20]

In this study, we have improved upon the poor processibility of polyaniline by copolymerizing it with *o*-anisidine, and melt processable conducting aniline/*o*-anisidine copolymer doped with superfluous DBSA was achieved by emulsion polymerization and hot doped technique. The conducting composites of aniline/*o*-anisidine copolymer/LLDPE with ethylene–acrylic acid copolymer (EAA) as compatibilizer were prepared by melt processing. The electrical and mechanical properties, resistivity-temperature characteristic, and morphology of the composites also were investigated.

EXPERIMENTAL

Materials

Aniline (Ani) and *o*-anisidine (oAs) of analytical grade were purchased from Shanghai Chemical Reagent and

Correspondence to: G. Wang (gengchaow@ecust.edu.cn).
Contract grant sponsor: National Natural Science Foundation of China; contract grant number: 20236020.
Contract grant sponsor: Shanghai Municipal Science and Technology Commission; contract grant numbers: 0352nm052, 04DZ14002.
Contract grant sponsor: Development Project of Shanghai Priority Academic Discipline.

© 2005 Wiley Periodicals, Inc.

distilled under vacuum prior to use. Ammonium persulfate, hydrochloric acid, chloroform, xylene, and DBSA of analytical grade were used without further purification. LLDPE (MFI = 2.0 g/10 min at 190 °C) was supplied by Qilu Petrochem (China), EAA (9.7 wt % acrylic acid; MFI = 1.5 g/10 min at 190 °C) was obtained from Dow Chemical.

Synthesis of conducting P(An-*co*-oAs)–DBSA

An amount of 6.5 g (70.0 mmol) of aniline, 3.7 g (30.0 mmol) of *o*-anisidine, and 17.5g DBSA was injected in 200 mL mixed solution of chloroform and deionized water (1/1, v/v) with stirring. A total of 25.1 g (110.0 mmol) of ammonium persulfate (dissolved in 100 mL deionized water) was dropped into the emulsion during stirring at 5 °C. The emulsion polymerization was allowed to proceed for 24 h at 5 °C. The protonated aniline/*o*-anisidine copolymer was obtained and then converted to the emeraldine base (EB) form by treatment with 10 wt % of aqueous ammonia solution for 24 h. ^{1}H-NMR spectrum analysis of the P(An-*co*-oAs) has shown a molar ratio aniline/*o*-anisidine of 0.57/0.43.

Redoping of the aniline/*o*-anisidine copolymer EB with DBSA was performed by mixing the EB with DBSA in a molar ratio of 1 : 0.9 in xylene at 75 °C for 8 h. After being dried, conducting aniline/*o*-anisidine copolymer (P(An-*co*-oAs)-DBSA) was obtained, of which the electrical conductivity of P(An-*co*-oAs)-DBSA is 13.7 S/cm.

Preparation of P(An-*co*-oAs)-DBSA/LLDPE/EAA and P(An-*co*-os)-DBSA/LLDPE composites

LLDPE and EVA were blended with P(An-*co*-oAs)–DBSA in various proportions on a two-roll mill at 140 °C for 10 min. Sheets of about 1.0-mm thickness of the conducting composites can be obtained by compression molding at 120 °C for 1min. The sheets were annealed at 105 °C for 24 h.

Measurements

The electrical conductivity of the samples was measured with a four-probe method. For resistivity-temperature testing, the sheets were cut into specimens of diameter 13 mm and coated with thin silver paint to reduce specimen–electrode contact resistance. The resistivity tester was constructed according to ISO3915–1999, equipped with thermostatic devices. The measurement of resistivity was conducted in the thickness direction of the specimen at a heating rate of 3 °C/min, using a digital multimeter. The UV–vis-NIR spectra were recorded on a Varian Cary 500 NIR spectrophotometer. For SEM analysis, samples were fractured under liquid nitrogen, and the surfaces were coated with a gold vapor. Micrographs were taken with a Jeol JSM–6360 scanning electron microscope. X–ray diffraction (XRD) patterns were obtained using a Rigaku D/Max 2550 VB/PC X-ray diffractometer possessing CuKα radiation. The diffraction data were recorded for 2θ angles between 3 and 60°. Differential scanning calorimetry (DSC) thermograms were taken on a Netzsch DSC 200PC thermal analyzer, operating under nitrogen atmosphere at 10 °C/min, from 20 to 200 °C. Mechanical properties were performed on a WSM-20kN at 25 °C with a crosshead speed of 250 mm/min. These specimens were cut by the standard ASTM D638 method.

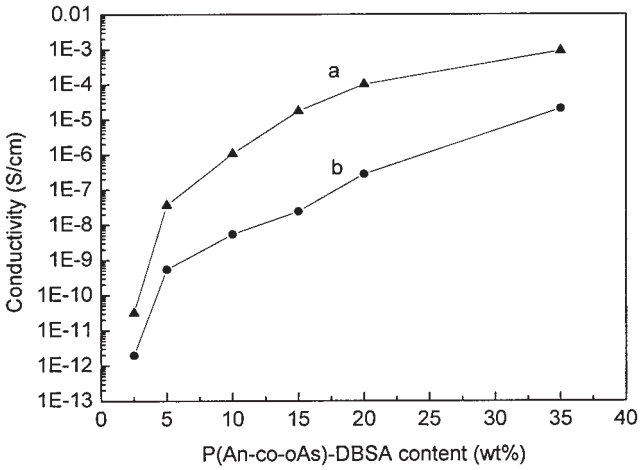

Figure 1 Electrical conductivity versus P(An-*co*-oAs)-DBSA content for (a) P(An-*co*-oAs)-DBSA/(LLDPE/EAA 70/30) and (b) P(An-*co*-oAs)-DBSA/LLDPE.

RESULTS AND DISCUSSION

Conductivity

The dependence of the conductivity on the P(An-*co*-oAs)-DBSA content for the P(An-*co*-oAs)-DBSA/LLDPE binary and P(An-*co*-oAs)-DBSA/LLDPE/EAA ternary composites is illustrated in Figure 1. For the P(An-*co*-oAs)-DBSA/LLDPE binary composite and P(An-*co*-oAs)-DBSA/LLDPE/EAA ternary composite, the percolation threshold all occurs at around 5 wt %, but the conductivity of P(An-*co*-oAs)-DBSA/LLDPE/EAA (10/63/21) ternary composite reaches 3.63 $\times$ 10^{-8} S/cm, which has an increase of 2 magnitudes more than that of P(An-*co*-oAs)-DBSA/LLDPE binary. Beyond percolation, the conductivity level slowly increases with increase of the P(An-*co*-oAs)-DBSA content, due to the generation of a conductive network of improved quality. The conductivity for P(An-*co*-oAs)-DBSA/LLDPE/EAA and P(An-*co*-oAs)-DBSA/LLDPE at 35 wt % of P(An-*co*-oAs)-DBSA content, respectively, attains 9.05 $\times$ 10^{-4} S/cm and 2.02 $\times$ 10^{-5} S/cm. This indicates that the electrical conductivity of

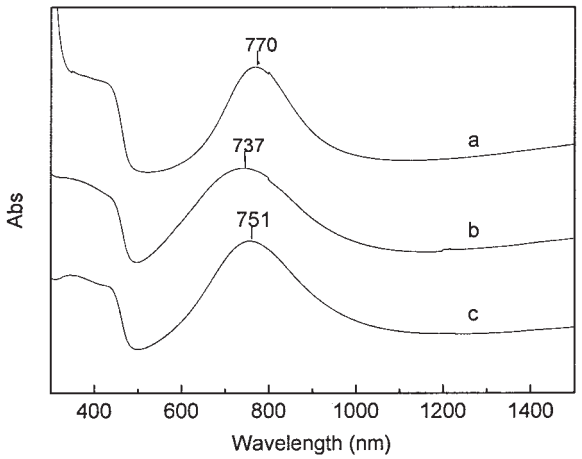

Figure 2 UV–vis-NIR spectra for (a) P(An-*co*-oAs)–DBSA, (b)P(An-*co*-oAs)-DBSA/LLDPE = 10/90, and (c) P(An-*co*-oAs)-DBSA/LLDPE/EAA = 10/63/27.

ternary composites markedly increases owing to the introduction of EAA.

UV–vis-NIR spectra analysis

The UV–vis-NIR spectra of P(An-*co*-oAs)-DBSA, P(An-*co*-oAs)-DBSA/LLDPE, and P(An-*co*-oAs)-DBSA/LLDPE/EAA composites are shown in Figure 2. The UV–vis-NIR spectrum of P(An-*co*-oAs)-DBSA [Fig. 2(a)] exhibits an absorption peak at 770 nm, which can be assigned to the polaron/bipolaron band transition. For P(An-*co*-oAs)-DBSA/LLDPE binary composite [Fig. 2(b)], the polaron/bipolaron band appears as an obvious blue shift from 770 to 737 nm, which indicates that the dedoping process of P(An-*co*-oAs)-DBSA may have taken place during melt blending. The TGA measurement for P(An-*co*-oAs)-DBSA supports this interpretation, as shown in Figure 3. The weight loss between 230 and 410 °C corresponded to the degradation of the bound DBSA and also free DBSA.[15] The weight loss above 410 °C is attributed mainly to decomposition of the P(An-*co*-oAs). At melt processing, the high temperature occurred duo to the high shear stress, resulting in dedoping of P(An-*co*-oAs)-DBSA. However, for the P(An-*co*-oAs)-DBSA/LLDPE/EAA ternary composite [Fig. 2(c)], the polaron/bipolaron band exhibits little blue shift, which suggests that the presence of EAA may restrain the dedoping of P(An-*co*-oAs)-DBSA due to protonation effect of carboxylic groups in EAA.

Morphological analysis

The effect of EAA on the morphology of the P(An-*co*-oAs)-DBSA/LLDPE composite was investigated by SEM. Figure 4 illustrates the SEM micrographs of the cryogenically fractured surfaces of the P(An-*co*-oAs)-DBSA/LLDPE [Fig. 4(a)] and P(An-*co*-oAs)-DBSA/LLDPE/EAA [Fig. 4(b)]. The conducting phase is shown as the light areas in the micrographs.

As shown in Figure 4(a), the P(An-*co*-oAs)-DBSA particles with diameters of 200–300 nm were dispersed in the LLDPE matrix for binary composite and the discontinuous conducting paths are observed, which agrees with the lower electrical conductivity in binary composite. This suggests that the compatibility between the LLDPE and conducting P(An-*co*-oAs)-DBSA is bad. In ternary composites (see Fig. 4(b)), the fibrillar-like P(An-*co*-oAs)-DBSA exists in the LLDPE matrix due to the introduction of EAA. Continuous conducting networks are formed, which results in higher conductivity for the ternary composite.

Crystallinity and melting behavior

X-ray diffraction patterns of P(An-*co*-oAs)-DBSA, LLDPE/EAA, P(An-*co*-oAs)-DBSA/LLDPE, and P(An-*co*-oAs)-DBSA/LLDPE/EAA are presented in Figure 5. P(An-*co*-oAs)-DBSA exhibits two weak and broad reflections at $2\theta = 20^{o}$ and 25^{o}, which indicates that P(An-*co*-oAs)-DBSA is an amorphous structure (see Fig. 5(a)). The LLDPE/EAA matrix reveals two strong reflections at $2\theta = 21^{o}$ and 24^{o}, which correspond to the 110 and 200 of LLDPE, respectively (see Fig. 5(b)).[21]

P(An-*co*-oAs)-DBSA/LLDPE and P(An-*co*-oAs)-DBSA/LLDPE/EAA exhibit typical reflections of LLDPE at similar angles (see Fig. 5(c,d)). The lattice spacing of P(An-*co*-oAs)-DBSA/LLDPE/EAA is basically in accord with the crystallization data of the LLDPE/EAA matrix (see Table I). Table I shows that the crystal structure for LLDPE is not destroyed after P(An-*co*-oAs)-DBSA is introduced. This suggests that P(An-*co*-oAs)-DBSA is dispersed within the amorphous regions of LLDPE instead of the crystalline regions.[22]

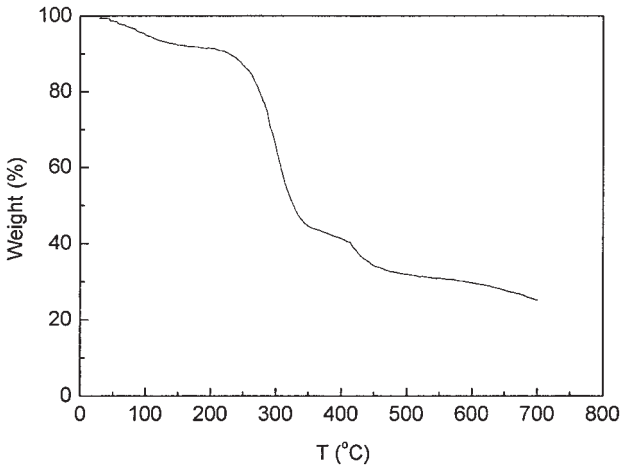

Figure 3 TGA thermogram of P(An-*co*-oAs)-DBSA.

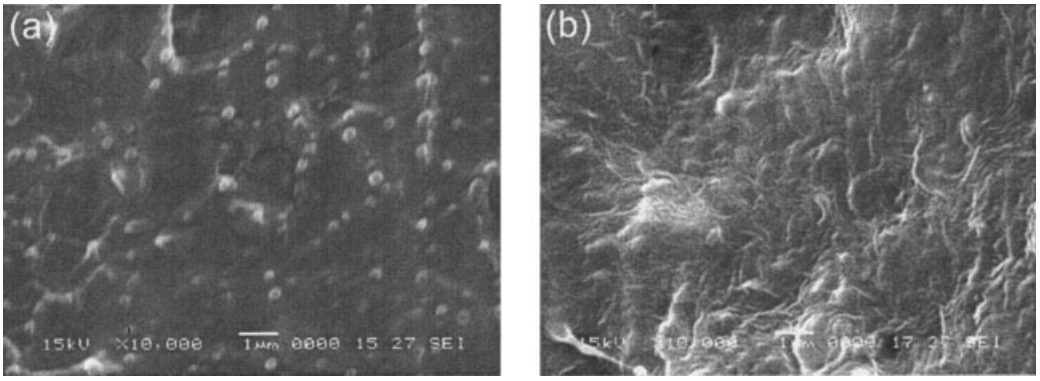

Figure 4 SEM micrographs for (a) P(An-*co*-oAs)-DBSA/LLDPE = 20/80 and (b) P(An-*co*-oAs)-DBSA/LLDPE/EAA = 20/56/24.

The DSC thermograms for P(An-*co*-oAs)-DBSA, LLDPE/EAA, P(An-*co*-oAs)-DBSA/LLDPE, and P(An-*co*-oAs)-DBSA/LLDPE/EAA are given in Figure 6. P(An-*co*-oAs)-DBSA exhibits a broad endothermic peak between 50 and 170 °C, corresponding to the small weight loss of water and oligomers.[23] From Figure 6(b), it is seen that the LLDPE/EAA matrix reveals two obvious endothermic peaks, which assign to the crystalline melt for LLDPE.[22] For P(An-*co*-oAs)-DBSA/LLDPE and P(An-*co*-oAs)-DBSA/LLDPE/EAA, the endothermic peaks of LLDPE also are observed and changed little after the introduction of P(An-*co*-oAs)-DBSA. This indicates that the crystal structure for LLDPE is not changed.

Resistivity-temperature characteristic

The curves of log ρ versus temperature for P(An-*co*-oAs)-DBSA/LLDPE and P(An-*co*-oAs)-DBSA/LLDPE/EAA are shown in Figure 7. From Figure 7, it can be seen that the log ρ of P(An-*co*-oAs)-DBSA/LLDPE and P(An-*co*-oAs)-DBSA/LLDPE/EAA slowly increases in the range of 25 to 70 °C. After 70 °C log ρ obviously increases with the increase of temperature. When the temperature rises to about 110 °C, log ρ approaches its maximum, and the positive temperature coefficient (PTC) characteristic occurs. However, the resistivity sharply drops after the temperature exceeds the maximum peak of log ρ. The resistivity again rises after about 125 °C. It is mainly related to thermal deprotonation of DBSA, as shown in Figure 8.

The resistivity-temperature characteristic of P(An-*co*-oAs)-DBSA/LLDPE and P(An-*co*-oAs)-DBSA/LLDPE/EAA correlates with microstructure and crystal melting behavior. The conductivity of the composites mainly depends on the gaps between the P(An-*co*-oAs)-DBSA particles. At room temperature, P(An-*co*-oAs)-DBSA particles dispersed only in the amorphous region are compressed tightly, which results in lower resistivity. In the range from 25 to about 70 °C, the resistivity slow rises with the increase of temperature, due to the thermal expansion only in the amorphous region. When partial melting takes place after 70 °C, the resistivity begins to increase and the marked transition of a PTC curve begins to emerge. This is because the rapid expansion from crystalline to amorphous results in the rapid increase of gaps between the P(An-*co*-oAs)-DBSA particles. When the crystalline region is

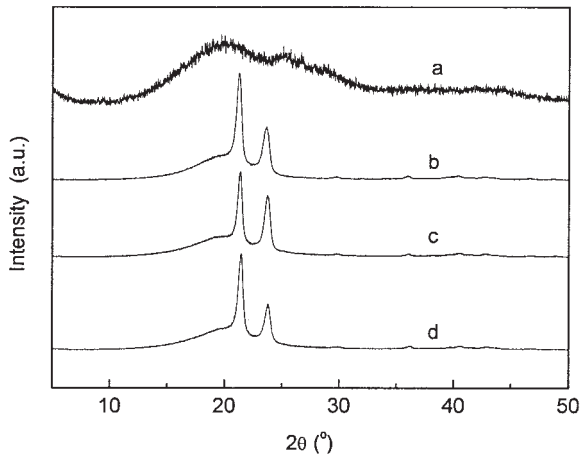

Figure 5 XRD patterns of (a) P(An-*co*-oAs)-DBSA, (b) LLDPE/EAA(70/30), (c) P(An-*co*-oAs)-DBSA/LLDPE = 20/80, and (d) P(An-*co*-oAs)-DBSA/LLDPE/EAA = 20/56/24.

TABLE I
The Lattice Distances for LLDPE/EAA, P(An-*co*-oAs)-DBSA/LLDPE, and P(An-*co*-oAs)-DBSA/LLDPE/EAA Composites

Composites	Lattice distances (nm)	
	110	200
LLDPE/EAA (70/30)	0.417	0.376
P(An-*co*-oAs)-DBSA/LLDPE/EAA = 20/56/24	0.413	0.374
P(An-*co*-oAs)-DBSA/LLDPE = 20/80	0.414	0.374

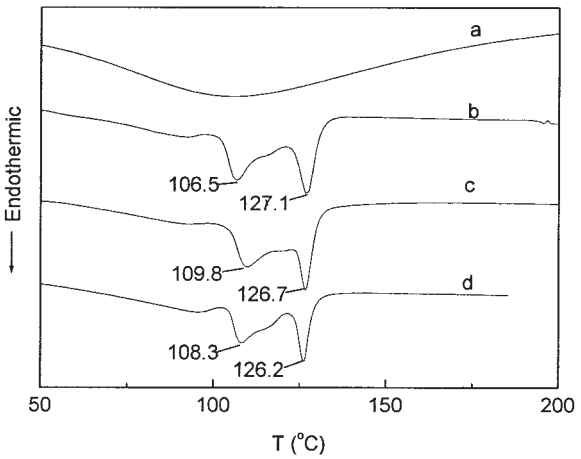

Figure 6 DSC curves of (a) P(An-*co*-oAs)-DBSA, (b) LLDPE/EAA(70/30), (c) P(An-*co*-oAs)-DBSA/LLDPE = 20/80, and (d) P(An-*co*-oAs)-DBSA/LLDPE/EAA = 20/56/24.

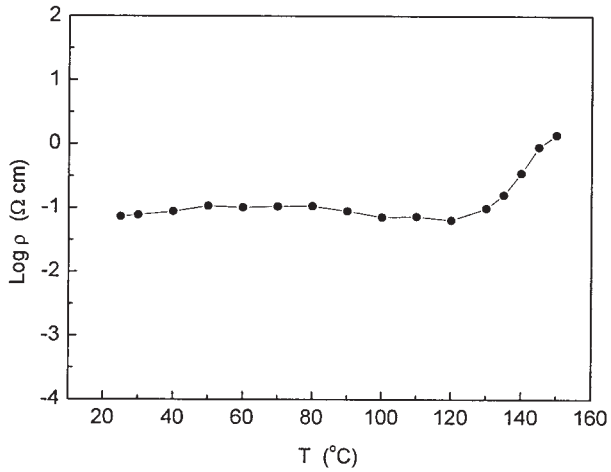

Figure 8 The dependence of log ρ on temperature for P(An-*co*-oAs)-DBSA.

fully melted, the gap between the P(An-*co*-oAs)-DBSA particles reaches its maximum. Figure 7 shows that the peak temperature of PTC curve is about 110 °C, which approximately coincides with the first endothermic peak temperature of the DSC curve. When the temperature exceeds the temperature at the peak of log ρ, the resistivity drops sharply (negative temperature coefficient, NTC). A possible explanation of the NTC, that above the melting point the reduction in ease of tunneling is counteracted by a further dispersion of the P(An-*co*-oAs)-DBSA particles, is similar to that of carbon black filled polyethylene composites.[24] The PTC intensity of P(An-*co*-oAs)-DBSA/LLDPE/EAA is weaker than that of P(An-*co*-oAs)-DBSA/LLDPE comparing Figure 7a with Figure 7b. This can be explained because the fibrillar-like continuous conducting networks of P(An-*co*-oAs)-DBSA/LLDPE/EAA are destroyed with more difficulty than the discontinuous conducting paths of P(An-*co*-oAs)-DBSA/LLDPE.

Mechanical properties

The stress–strain curves for LLDPE, LLDPE/EAA (70/30), P(An-*co*-oAs)-DBSA/LLDPE, and P(An-*co*-oAs)-DBSA/LLDPE/EAA are shown in Figure 9. The tensile strength and elongation at break of P(An-*co*-oAs)-DBSA/LLDPE and P(An-*co*-oAs)-DBSA/LLDPE/EAA composites as a function of the P(An-*co*-oAs)-DBSA content are given in Figure 10. The stress–strain behavior of P(An-*co*-oAs)-DBSA/LLDPE and P(An-*co*-oAs)-DBSA/LLDPE/EAA composites is like LLDPE because of the influence of the crystal phases of LLDPE. Both tensile strength and elongation at break decrease with the increase of P(An-*co*-oAs)-

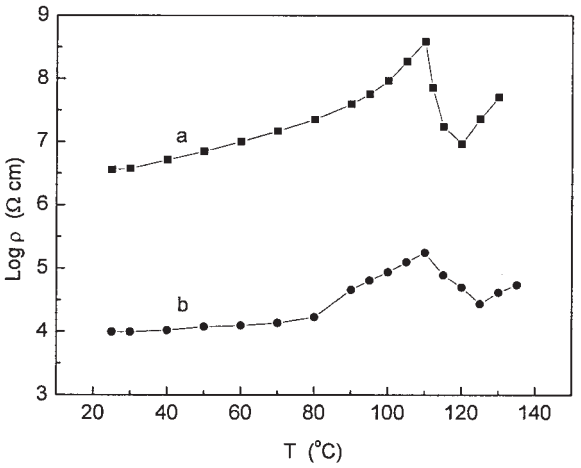

Figure 7 The dependence of log ρ on temperature in (a) P(An-*co*-oAs)-DBSA/LLDPE = 20/80 and (b) P(An-*co*-oAs)-DBSA/LLDPE/EAA = 20/56/24.

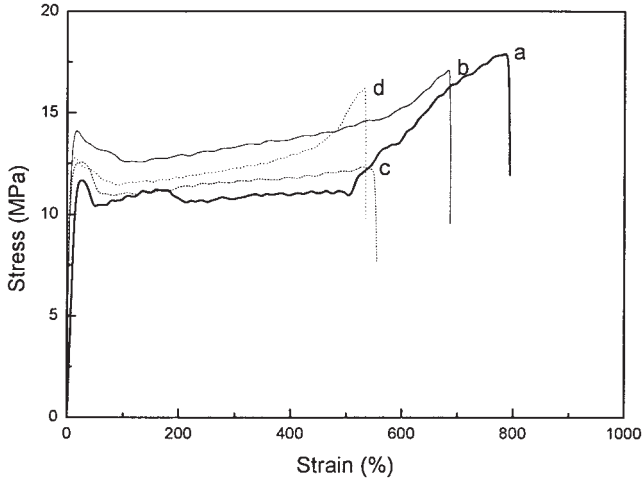

Figure 9 Stress–strain curves for (a) LLDPE, (b) LLDPE/EAA = 70/30, (c) P(An-*co*-oAs)-DBSA/LLDPE = 20/80, and (d) P(An-*co*-oAs)-DBSA/LLDPE/EAA = 20/56/24.

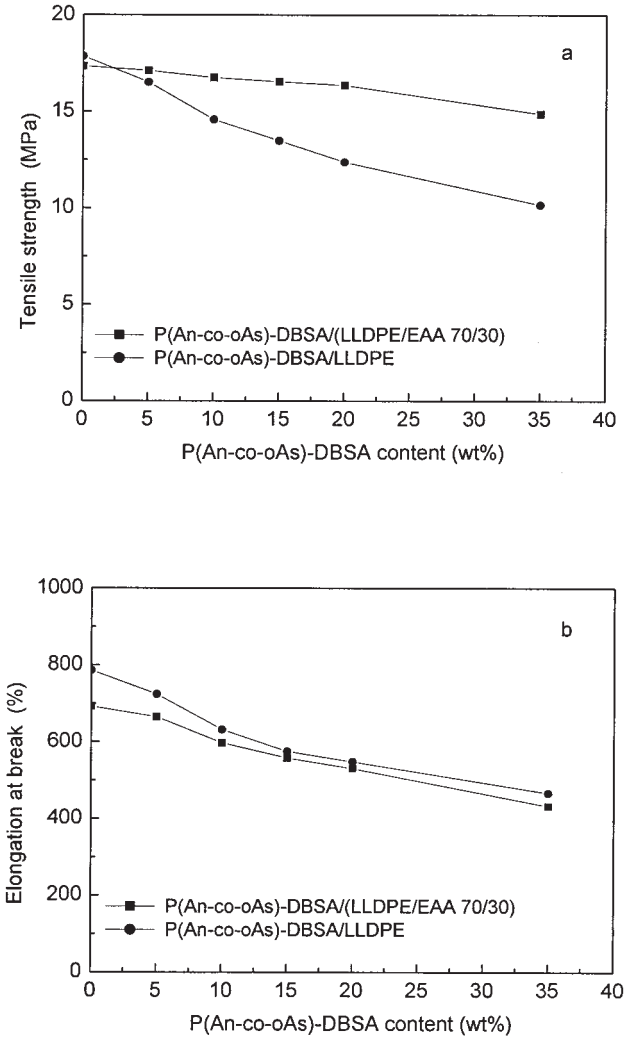

Figure 10 Effect of P(An-*co*-oAs)-DBSA content on the mechanical properties of conducting composites: (a) tensile strength and (b) elongation at break.

DBSA content, as a result of poor mechanical properties of the P(An-*co*-oAs)-DBSA caused by the presence of free DBSA. However, the descending extent of tensile strength for P(An-*co*-oAs)-DBSA/LLDPE/EAA composites is considerably less than that of P(An-*co*-oAs)-DBSA/LLDPE composites. This is because the fibrillar-like P(An-*co*-oAs)-DBSA as reinforcing agent is formed by the introduction of EAA in P(An-*co*-oAs)-DBSA/LLDPE/EAA composites, while the granular P(An-*co*-oAs)-DBSA occurred in P(An-*co*-oAs)-DBSA/LLDPE composites.

CONCLUSIONS

The conducting composites of aniline/*o*-anisidine copolymer doped by dodecylbenzenesulfonic acid (P(An-*co*-oAs)-DBSA), LLDPE, and EAA as compatibilizer were prepared by melt processing. The electrical conductivity, mechanical properties, resistivity-temperature characteristic, and morphological structure of the composites also were investigated. The electrical conductivity of ternary composites was markedly enhanced due to compatibilization and the protonation effect of the EAA. The SEM micrograph shows that the compatibility between the P(An-*co*-oAs)-DBSA and LLDPE matrix is enhanced due to introduction of EAA. The XRD and DSC results show that the crystalline structure of LLDPE/EAA did not change while P(An-*co*-oAs)-DBSA was added, and P(An-*co*-oAs)-DBSA was dispersed within the amorphous regions of LLDPE matrix. The PTC characteristic was also observed. The tensile strength of P(An-*co*-oAs)-DBSA/LLDPE/EAA composites was improved, compared with P(An-*co*-oAs)-DBSA/LLDPE composites. In addition, tensile strength and elongation at break of P(An-*co*-oAs)-DBSA/LLDPE and P(An-*co*-oAs)-DBSA/LLDPE/EAA all decreased with the increase of P(An-*co*-oAs)-DBSA content due to the presence of free DBSA.

References

1. Chang, J. C.; MacDiarmid, A. G. Synth Met 1986, 13, 193.
2. MacDiarmid, A. G.; Epstein, A. J Faraday Discuss Chem Soc 1989, 88, 317.
3. D'Aprano, G.; Leclerc, M.; Zotty, G.; Schiavon, G. Chem Mater 1995, 7, 33.
4. Zheng, W.-Y.; Levon, K.; Laakso, J.; Osterholm, J.-E. Macromolecules 1994, 27, 7754.
5. MaCoy, C. H.; Lorkovic, I. M.; Writon, M. S. J Am Chem Soc 1995, 117, 33.
6. Cao, Y.; Smith, P.; Heeger, A. J. Synth Met 1992, 48, 91.
7. Osterholm, J. E.; Cao, Y.; Klavetter, F.; Smith, P. Synth Met 1993, 55–57, 1034.
8. Cao, Y.; Smith, P. Polymer 1993, 34, 3139.
9. Laska, J.; Prón, A.; Lefrant, S. J. Polym Sci A Polym Chem 1995, 33, 1437.
10. Paul, R. K.; Vijayanathan, V.; Pillai, C. K. S. Synth Met 1999, 104, 189.
11. Paul, R. K.; Pillai, C. K. S. Synth Met 2000, 114, 27.
12. Ikkala, O. T.; Lindholm, T. M.; Ruohonenc, H.; Seläntausb, M.; Väkipartack, K. Synth Met 1995, 69, 135.
13. Anand, J.; Palaniappan, S.; Sathyanarayana, D. N. Prog Polym Sci 1998, 23, 993.
14. Ikkala, O. T.; Laakso, J.; Väkiparta, K.; Virtanen, E.; Ruohonen, H.; Järvinen, H.; Taka, T.; Passiniemi, P.; Österholm, J.-E. Synth Met 1995, 69, 97.
15. Barra, G. M. O.; Leyva, M. E.; Soares, B. G.; Mattoso, L. H.; Sens, M. J Appl Polym Sci 2001, 82, 114.
16. Zilberman, M.; Siegmann, A.; Narkis, M. J. Macromol Sci Phys 2000, B39(3), 333.
17. Faez, R.; De Paoli, M.-A. J Appl Polym Sci 2001, 82, 1768.
18. Yang, J. P.; Rannou, P; Planès, J; Proń, A.; Nechtschein, M. Synth Met 1998, 93, 169.
19. Laska, J.; Zak, K.; Prón, A. Synth Met 1997, 84, 117.
20. Tiltelman, G. I.; Zilberman, M.; Siegmann, A.; Haba, Y.; Narkis, M. J Appl Polym Sci 1997, 66, 2199.
21. Mo, Z. S. Synth Fibers 1981, 5, 65.
22. Luo, Y.-L.; Wang, G.-C.; Zhang, B.-Y.; Zhang, Z.-P Eur Polym Mater 1998, 34, 1221.
23. Zilberman, M.; Titelman, G. I.; Siegmann, A.; Haba, Y.; Narkis, M.; Alperstein, D. J Appl Polym Sci 1997, 66, 243.
24. Meyer, J. Polym Eng Sci 1974, 14, 706.